Elastic buckling mode decomposition of displacement, strain energy and stress components for thin-walled structural members

Junle Cai[1], Cristopher D. Moen[2]

Abstract

A buckling mode decomposition method of normalized displacement field, bending stresses and strain energy for thin-walled member displacement field (point clouds or finite element results) is introduced based on generalized beam theory (GBT). The method provides quantitative modal participation information regarding eigen-buckling displacement fields, stress components and elastic strain energy, that can be used to inform future design approaches. In the method, GBT modal amplitudes are retrieved at discrete cross-sections, and the modal amplitude field is reconstructed assuming it can be piece-wisely approximated by polynomials. The unit displacement field, stress components and strain energy are all retrieved by using reconstructed GBT modal amplitude field and GBT constitutive laws. Theory and examples are provided, and potential applications are discussed including cold-formed steel member design and post-disaster evaluation of thin-walled structural members.

1. Introduction

This paper introduces an elastic buckling mode decomposition method that provides unit displacements, bending stresses and strain energy of thin-walled structural members using Generalized Beam Theory (GBT). The method analyzes shell finite element analysis (SFEA) displacement fields and can be categorized as an inverse problem solution method. A typical GBT analysis calculates normalized displacements, stresses and strain energy, (Camotim et al., 2004) for elastic buckling and (Abambres et al., 2014) for plastic collapse directly for a thin-walled member. The method in this paper is different because it works backwards from any 3D deformation shape to quantify modal participation information.

---

[1]Ph.D. Candidate, Virginia Tech, <junlecai@vt.edu>
[2]Associate Professor, Virginia Tech, <cmoen@vt.edu>

Modal decomposition can be used to identify the dominant buckling mode for a SFEA solution, and then the solution can serve as input for current design approaches, for example the American Iron and Steel Institute's Direct Strength Method. From modal decomposition, modal contributions to key failure triggering quantities can be identified, e.g., stress, displacement, strain energy. For example, if the failure is initiated by excessive transverse bending, modal decomposition can reveal the contribution of the bending stress from short half-wave, local-plate buckling or longer wave, distortional buckling, and the design can be improved accordingly. The method proposed herein could also be applied to post-disaster evaluation of thin-walled structural members, where the displacement field, documented as a point cloud can be analyzed to determine its residual capacity.

Buckling mode identification methods have been developed based on GBT and constraint finite strip method (cFSM) on prismatic members. (Ádány et al., 2010) used cFSM basis function and conducted mode decomposition by reconstructing the displacement field in the cFSM basis space. (Li et al., 2013) documented the dominant deformation modes in simulations to collapse using cFSM decomposition method. (Nedelcu, 2012) used GBT stiffness matrices to calculate the modal participation with success. (Cai and Moen, 2015) brought out a modal decomposition method by using GBT mode shapes as basis functions to reconstruct the displacement field. The method is then employed in experiment to document the evolution of modal participation during collapse (Lama-Salomon et al., 2015). The extension made in this paper's method is that it applies on displacement field, stress components and strain energy, while the previous work are applicable on displacement field.

The modal decomposition method presented herein is based on GBT. The core concepts of GBT, including modal analysis and a system of ordinary differential equations (ODEs), were conceived by Schardt (Schafer, 2008), with the governing equations solved by the finite difference method when analytical solutions are not available. The finite element approach was developed for solving the GBT system of ODEs approximately (Silvestre and Camotim, 2003), which facilitated the application of GBT in buckling and dynamics problems. Shear modes that capture the shear lag effect and nonlinear longitudinal warping displacements can also be incorporated into GBT (Silvestre and Camotim, 2013), allowing the warping displacements in each fold line to be nonlinear (Ádány, 2014).

Modal identification methods for decomposing displacement, bending stress and strain energy are proposed that are inspired by the exising GBT body of knowledge. GBT modal amplitude at discrete cross-sections are retrieved (Cai and Moen, 2015) using out-of-plane displacements at discretization nodes read from shell finite element solution. The continuous modal amplitude field is reconstructed by assuming the modal amplitudes can be piece-wisely approximated by Hermite polynomials. Unit displacement, bending stress and strain energy are all retrieved by using reconstructed modal amplitude field and GBT constitutive laws. Methodology verification and examples are also provided.

2. Review: GBT elastic buckling analysis for thin-walled members

Consider a thin-walled prismatic member as shown in Figure 1 with the local coordinates system (x, s, z) and corresponding displacement components (u, v, w). In the context of generalized beam theory, the displacement field for the cross-section at length x is a linear combination of GBT mode

shapes

$$u(s,x) = u_k(s)\phi_{k,x}(x) \qquad v(s,x) = v_k(s)\phi_k(x) \qquad w(s,x) = w_k(s)\phi_k(x), \qquad (1)$$

where standard summation notation applies; $(\cdot), x = \partial(\cdot)/\partial x$; $u_k(s), v_k(s), w_k(s)$ are the functions specifying conventional GBT cross-sectional mode shapes; $\phi_k(x)$ is the modal amplitude vector of conventional GBT modes at length x along the member; ; and $u_k(s)\phi_{k,x}(x)$ in the first term stands for warping that arises from conventional GBT modes related to the first order derivatives of modal amplitudes. For conventional modes, Vlasov's null membrane strain assumption ($\varepsilon_{ss}^M = 0$, $\gamma_{xs}^M = 0$) is satisfied such that $v_k(s)$ is a constant in each fold line, and the warping function $u_k(s)$ varies linearly in each fold line.
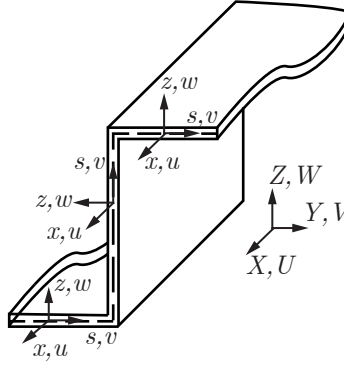

Figure 1: Coordinate system and translations for a thin-walled member.

The displacement field in Eq. (1) can also be written in the global system (X, Y, Z) and (U, V, W) as

$$U(s,x) = U_k(s)\phi_{k,x}(x) \qquad V(s,x) = V_k(s)\phi_k(x) \qquad W(s,x) = W_k(s)\phi_k(x), \qquad (2)$$

where (U, V, W) and $U_k(s)$, $V_k(s)$, $W_k(s)$ are displacements and GBT modes shapes in the global coordinate system. To determine the GBT mode shapes $u_k(s), v_k(s), w_k(s)$ or equivalently $U_k(s)$, $V_k(s), W_k(s)$, the cross-section is discretized by 'natural nodes' and 'intermediate nodes', and GBT 'cross-sectional analysis' is carried out. The 'cross-sectional analysis' derivation is complex and lengthy. One may refer to (Dinis and Camotim, 2011; Schardt, 1989; Gonçalves et al., 2010) for determination of GBT modes. The most relevant conventional mode shapes for a Cee-section are shown in Figure 2a-c.
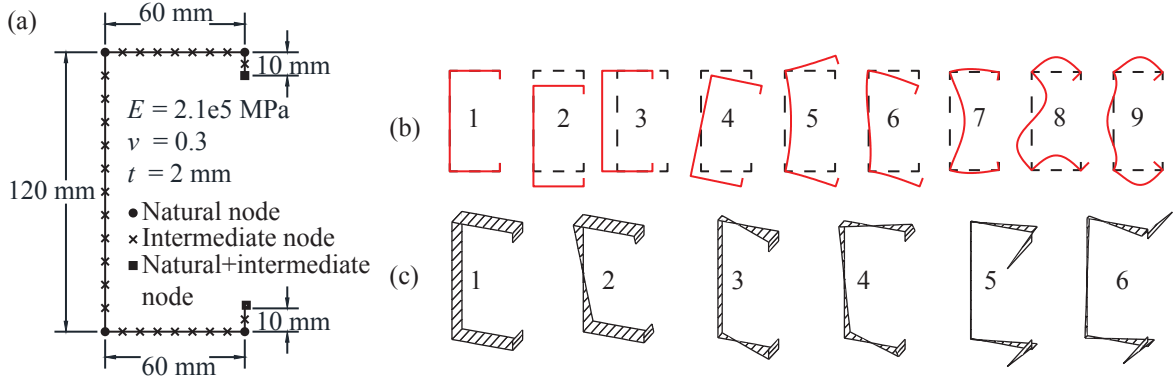
Figure 2: GBT mode shapes: (a) cross-section dimensions and discretization; (b) in-plane components of GBT modes; (c) warping components of GBT modes.

The GBT formulation employs Kirchhoff-Love plate theory and strains, in which are related to displacement components as

$$
\begin{aligned}
\varepsilon_{xx} &= u_{,x} = (u_k - z w_k)\phi_{k,xx}, \\
\varepsilon_{ss} &= v_{,s} = -z w_{k,ss}\phi_k, \\
\gamma_{xs} &= u_{,s} + v_{,x} = (u_{k,s} + v_k)\phi_{k,x} - 2z w_{k,s}\phi_{k,x} + u_{j,s}\varphi_j, \\
\varepsilon_{xx}^{NL} &= (v_{,x}^2 + w_{,x}^2)/2 = (v_i\phi_{i,x}v_k\phi_{k,x} + w_i\phi_{i,x}w_k\phi_{k,x})/2,
\end{aligned}
\tag{3}
$$

in which ε_{xx}^{NL} stands for the nonlinear normal stain component essential for forming the geometric stiffness matrix. Stress components are related to strains by the constitutive law

$$
\begin{Bmatrix} \sigma_{xx}^M \\ \sigma_{xx}^F \\ \sigma_{ss}^F \\ \tau_{xs} \end{Bmatrix} =
\begin{bmatrix}
E & 0 & 0 & 0 \\
0 & \frac{E}{1-\nu^2} & \frac{\nu E}{1-\nu^2} & 0 \\
0 & \frac{\nu E}{1-\nu^2} & \frac{E}{1-\nu^2} & 0 \\
0 & 0 & 0 & G
\end{bmatrix}
\begin{Bmatrix} \varepsilon_{xx}^M \\ \varepsilon_{xx}^F \\ \varepsilon_{ss}^F \\ \tau_{xs} \end{Bmatrix},
\tag{4}
$$

where E, ν, G are elastic modulus, Poisson's ratio, and shear modulus, respectively; and $\sigma_{ij}, \varepsilon_{ij}$ are stress and strain components, $(\cdot)^M$ denotes membrane terms and $(\cdot)^F$ denotes frexural term. The GBT differential equation system of equilibrium can be derived by using the Principle of Virtual Work and it reads

$$
C_{ik}\frac{\partial^4 \phi_k}{\partial x^4} - (D_{ik}^I - D_{ik}^{II} - D_{ki}^{II})\frac{\partial^2 \phi_k}{\partial x^2} + B_{ik} - W_p^0 X_{pik}\frac{\partial^2 \phi_k}{\partial x^2} = q_i^{II} - q_{i,x}^I,
\tag{5}
$$

where subscripts i, k correspond to conventional GBT modes. Tensors denoted by C, D and X are calculated using GBT mode shapes, cross-sectional dimensions and material properties:

$$
C_{ik} = \int_b E u_i u_k ds + \int_b \frac{Et^3}{12(1-\nu^2)} w_i w_k ds, \qquad D_{ik}^I = \int_b \frac{Gt^3}{3} w_{i,s} w_{k,s} ds,
$$

$$
D_{ik}^{II} = \int_b \frac{\nu Et^3}{12(1-\nu^2)} w_i w_{k,ss} ds, \qquad B_{ik} = \int_b \frac{t^3}{12(1-\nu^2)} w_{i,ss} w_{k,ss} ds.
$$

4

X_{pik} is a third order tensor defined by:

$$X_{pik} = \int_b E \frac{u_p}{C_{pp}} (v_i v_k + w_i w_k) ds. \tag{6}$$

where u_p is the pth GBT mode shape (warping) corresponding to axial compression ($p = 1$), major axis bending ($p = 2$), minor axis bending ($p = 3$), and torsional warping ($p = 4$); and C_{pp}/E is the cross-sectional property of area ($p = 1$), major axis moment of inertia ($p = 2$), minor axis moment of inertia ($p = 3$), warping moment of inertia ($p = 4$). q_i^I, q_i^{II} are force vectors correspond to GBT modes who stems from traction q_x, q_s, and q_z along the local coordinate axes x, s, z (Figure 1) applied at the center line of the thin plate, they are:

$$q_i^I = \int_b q_x u_i ds \qquad\qquad q_i^{II} = \int_b (q_s v_i + q_z w_i) ds. \tag{7}$$

Eq. (5) is an ordinary differential equations with unknowns being ϕ_k. With boundary conditions defined, this system can be piece-wise approximately solved by the finite element method. The functions $\phi_k(x)$ (conventional modes except axial extension) are approximated by Hermite polynomials

$$\phi_k = \psi_1 d_{k.1} + \psi_2 d_{k.2} + \psi_3 d_{k.3} + \psi_4 d_{k.4}. \tag{8}$$

The function $\phi_{1,x}(x)$ (axial extension mode) is approximated by Lagrange polynomials

$$\phi_{1,x} = \zeta_1 d_{1.1} + \zeta_2 d_{1.2} + \zeta_3 d_{1.3} + \zeta_4 d_{1.4}. \tag{9}$$

In Eq. (8) and Eq. (9) ψ_{1-4} and ζ_{1-4} are shape functions of Hermite and Lagrange polynomials as shown in Eq. (10) and Figure 3; and $d_{k.r}$ stands for the rth FE degree of freedom in the approximation of kth modal amplitude also shown in Figure 3.

$$\Psi = \left\{ \tfrac{1}{2}(1 - \xi)(3\xi - 1)(3\xi - 2) \quad \tfrac{9}{2}\xi(\xi - 1)(3\xi - 1) \quad \tfrac{9}{2}\xi(1 - \xi)(3\xi - 2) \quad \tfrac{1}{2}\xi(3\xi - 1)(3\xi - 2) \right\},$$
$$Z = \left\{ L_e(\xi^3 - 2\xi^2 + \xi) \quad 2\xi^3 - 3\xi^2 + 1 \quad L_e(\xi^3 - \xi^2) \quad -2\xi^3 + 3\xi^2 \right\},$$
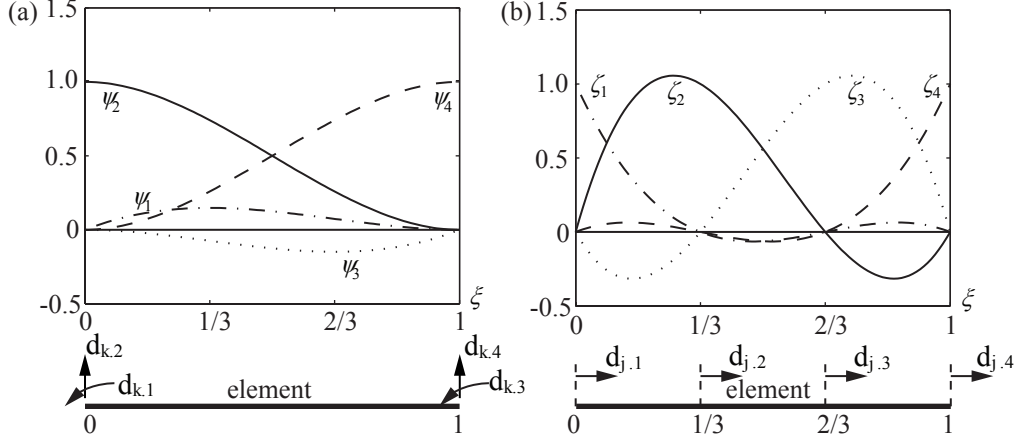$$\tag{10}$$

Figure 3: Shape functions and FE degrees of freedom of (a) Hermite polynomials; (b) Lagrange polynomials.

In the linear stability analysis, the FE eigen-buckling problem is defined as

$$\left(\begin{bmatrix} \mathbf{k}_{11} & \mathbf{0} \\ \mathbf{0} & \mathbf{k}_{ik} \end{bmatrix} + \lambda \begin{bmatrix} \mathbf{0} & \mathbf{0} \\ \mathbf{0} & \mathbf{g}_{ik} \end{bmatrix} \right) \begin{Bmatrix} \mathbf{d}_1 \\ \mathbf{d}_k \end{Bmatrix} = \begin{Bmatrix} \mathbf{0} \\ \mathbf{0} \end{Bmatrix}, \tag{11}$$

where $\mathbf{k}$ is the symmetric linear stiffness matrix contains 2 sub-matrices $\mathbf{k}_{11}$, $\mathbf{k}_{ik}$ reading

$$\mathbf{k}_{11} = C_{11} \int_{Le} Z'^T Z' dx,$$
$$\mathbf{k}_{ik} = C_{ik} \int_{Le} \Psi''^T \Psi'' dx + D_{ik}^I \int_{Le} \Psi'^T \Psi' dx + D_{ik}^{II} \int_{Le} \Psi''^T \Psi dx + D_{ki}^{II} \int_{Le} \Psi^T \Psi'' dx + B_{ik} \int_{Le} \Psi^T \Psi dx,$$
$$\tag{12}$$

In Eq. (12), 1 stands for the uniform compression mode, i, k for the other conventional modes. The sub-matrices in geometric stiffness $\mathbf{g}$ have values

$$\mathbf{g}_{ik} = W_p X_{pik} \int_{Le} \Psi'^T \Psi' dx, \tag{13}$$

3. Buckling Mode Decomposition of Displacement, Strain Energy and Bending Stress Components

3.1. Reconstruction of GBT modal amplitude field

In (Cai and Moen, 2015), an algorithm for retrieving the modal amplitudes at discrete cross-sections from finite element displacement field or experimental point cloud was introduced. The modal amplitudes at a given cross-section can be found by solving the least squares problem in Eq. (14):

$$\sum_{k=2}^{n} \begin{bmatrix} V_k \\ W_k \end{bmatrix}_{2n \times (n+1)} \{\phi_k(x)\}_{(n+1) \times 1} \overset{\substack{least \\ square}}{=} \begin{Bmatrix} V \\ W \end{Bmatrix}_{2n \times 1}, \tag{14}$$

in which (i) V_k, W_k are displacement components at discretization nodes of GBT mode k in the

global coordinate system; (ii) $\phi_k(x)$ is the modal amplitude vector of mode k at location x along the member, (iii) V, W are out-of-plane displacements in the global coordinate system (Figure 1) obtained by FEA or by test measurements, (iv) the subscript denotes the dimensions of the matrix with n being the number of discretization nodes.

By retrieving the modal amplitudes at discrete cross-section, the out-of-plane displacement - (v, w) or (V, W) in Figure 1 - can be decomposed into modal contributions by knowing Eq. (1) and Eq. (2). The objectives of this paper include the decomposition of displacement, strain energy and bending stress regarding the contribution from GBT modes. From Eq. (2), Eq. (4) and Eq. (12), that requires the full information of modal amplitude variation. To reconstruct modal amplitude field, it is assumed $\phi_k(x)$ can be piece-wisely approximated by polynomials like shown in Eq. (8). The member is divided into several sub-domains each containing 4 discrete cross-sections, as shown in Figure 4. Because Hermitian polynomial is used to approximate $\phi_k(x)$, Eq. (8) applies and

$$
\begin{aligned}
\phi_k(0) &= \psi_1(0)d_{k.1} + \psi_2(0)d_{k.2} + \psi_3(0)d_{k.3} + \psi_4(0)d_{k.4}, \\
\phi_k(1/3L^e) &= \psi_1(1/3L^e)d_{k.1} + \psi_2(1/3L^e)d_{k.2} + \psi_3(1/3L^e)d_{k.3} + \psi_4(1/3L^e)d_{k.4}, \\
\phi_k(2/3L^e) &= \psi_1(2/3L^e)d_{k.1} + \psi_2(2/3L^e)d_{k.2} + \psi_3(2/3L^e)d_{k.3} + \psi_4(2/3L^e)d_{k.4}, \\
\phi_k(L^e) &= \psi_1(L^e)d_{k.1} + \psi_2(L^e)d_{k.2} + \psi_3(L^e)d_{k.3} + \psi_4(L^e)d_{k.4},
\end{aligned}
\tag{15}
$$

where L^e denotes the domain under consideration; $\phi_k(\alpha L^e)$ is modal amplitude calculated by Eq. (14) at αL^e; $\psi_i(\alpha L^e)$ corresponds to the value of ith Hermitian shape function (Eq. (8), Figure 3) at the location αL^e; $d_{k,i}$ denotes the ith FE degree-of-freedom of the kth GBT mode (Eq. (8), Figure 3). d_k can be solved for by using Eq. (16) and the continuous distribution of ϕ_k is approximated. The concept is depicted in Figure 4.

$$
\begin{Bmatrix} d_{k.1} \\ d_{k.2} \\ d_{k.3} \\ d_{k.4} \end{Bmatrix} = \begin{bmatrix} \psi_1(0) & \psi_2(0) & \psi_3(0) & \psi_4(0) \\ \psi_1(1/3L^e) & \psi_2(1/3L^e) & \psi_3(1/3L^e) & \psi_4(1/3L^e) \\ \psi_1(2/3L^e) & \psi_2(2/3L^e) & \psi_3(2/3L^e) & \psi_4(2/3L^e) \\ \psi_1(L^e) & \psi_2(L^e) & \psi_3(L^e) & \psi_4(L^e) \end{bmatrix}^{-1} \begin{Bmatrix} \phi_k(0) \\ \phi_k(1/3L^e) \\ \phi_k(2/3L^e) \\ \phi_k(L^e) \end{Bmatrix}.
$$

(16)

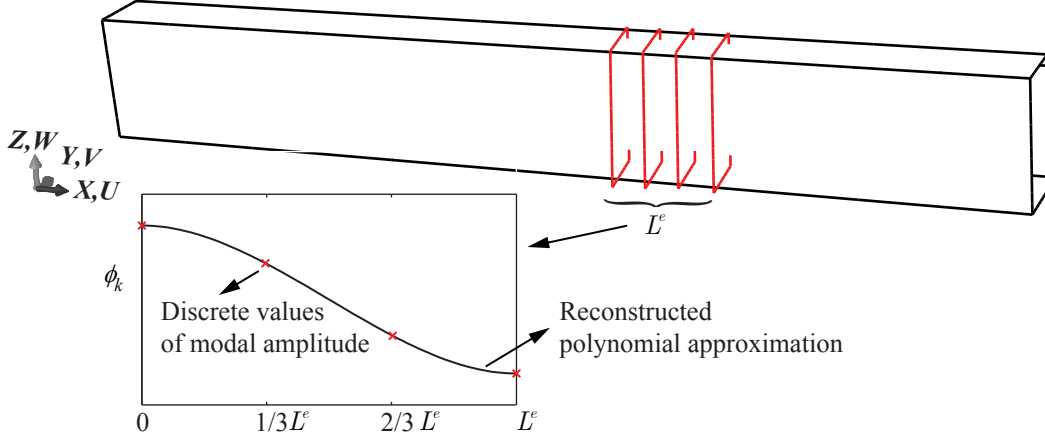Figure 4: Concept of using polynomials to piece-wisely approximate the modal amplitude ϕ_k.

3.2. Decomposition of strain energy and bending stresses

The energy stored in the interaction of GBT mode i and k is

$$E_{ik} = \frac{1}{2}d_i k_{ik} d_k, \tag{17}$$

where k_{ik} stands for the linear, interactive stiffness matrix of mode i and k as shown in Eq. (12); d_i, d_k are the finite element degree of freedom vectors for the domain where piece-wise approximation is applied. Obviously E_{ii} stands for the energy stored in mode i. And the strain energy in total is

$$E_{total} = \sum_i \sum_k E_{ik}. \tag{18}$$

Strain energy can be used as an ambiguous modal participation indicator because the strain energy distribution is independent with the GBT mode normalization. The transverse and longitudinal bending stress, according to Eq. (1), Eq. (3), Eq. (4), are

$$\sigma_{ss}^F(x,s,t) = \frac{E}{1-\nu^2}w_{k,ss}(s,t)\phi_k(x) + \frac{\nu E}{1-\nu^2}w_k(s,t)\phi_{k,xx}(x), \tag{19}$$

$$\sigma_{xx}^F(x,s,t) = \frac{\nu E}{1-\nu^2}w_{k,ss}(s,t)\phi_k(x) + \frac{E}{1-\nu^2}w_k(s,t)\phi_{k,xx}(x), \tag{20}$$

where summation convention applies; $\sigma_{ss}^F, \sigma_{xx}^F$ denotes transverse and longitudinal bending stresses respectively; w_k is plate transverse deflection component of the kth GBT mode shape as in Eq. (1), and ϕ_k is the kth GBT mode amplitude that can be obtained by using d_k and Eq. (8).

3.3. Evaluation of reconstructed displacement field error

The error of the reconstructed displacement field can be evaluated by

$$error = \sqrt{\frac{\sum[(V_{SFEA} - V_{reconstructed})^2 + (W_{SFEA} - W_{reconstructed})^2]}{\sum(V_{SFEA}^2 + W_{SFEA}^2)}}, \tag{21}$$

8

where $\sum$ means it applies to all the discretization nodes; V_{SFEA}, W_{SFEA} are out-of-plane displacement components read from shell finite element solution; $V_{reconstructioned}, W_{reconstructed}$ are reconstructed displacement components calculated by using $\phi_{k-reconstructed}$ and Eq. (2).

3.4. Cross-sectional modal participation calculation

Cross-sectional modal displacement participation is calculated as

$$P_k = \frac{\int_L |g_k \phi_k(x)| dx}{\sum\limits_{k=1}^{n} \int_L |g_k \phi_k(x)| dx}, \tag{22}$$

where $g_k = r_g$ for torsional cross-section modes (e.g., mode 4 in Figure 2) and $g_k = 1$ for all other modes. This approach converts member twist in radians to a cross-section displacement so that it can be compared to the other displacement-based mode shapes. The conversion from radians to displacement is performed by multiplying ϕ_4 by the radius of gyration, r_g, calculated about the cross-section center of twist, i.e., the shear center,

$$r_g = \sqrt{r_1^2 + r_2^2}, \quad r_1 = \sqrt{I_1/A}, \quad r_2 = \sqrt{I_2/A}, \tag{23}$$

where I_1 and I_2 are moment of inertia about the principal axes with origin at the cross-section center of twist and A is the cross-sectional area. This approach is different than other modal participation factor approaches that combine displacement and twist together (Silvestre and Camotim, 2002).

4. Illustrative examples

4.1. Example I

The derivation above is applicable on eigen-buckling solutions. In order to show the results, the eigen-buckling solutions are normalized in the following examples such that maximum displacement is unity, i.e.,

$$\max \left(\sqrt{U_{FE}^2 + V_{FE}^2 + W_{FE}^2} \right) = 1. \tag{24}$$

The first example is a $870\,mm$ long member with the cross-section shown in Figure 2. The member is warping-fixed at the left end and pinned-warping fixed at the right, and loaded with a compressive traction q at the pinned-warping free end. For shell finite-element modeling in ABAQUS, the discretization is identical with GBT in the cross-sectional directions, as shown in Figure 2. In longitudinal direction, the discretization is made every $10mm$. The lowest buckling load is $146.4kN$ and the out-of-plane displacements (V, W in Figure 1) of all the discretization nodes are read from ABAQUS for modal decomposition analysis.
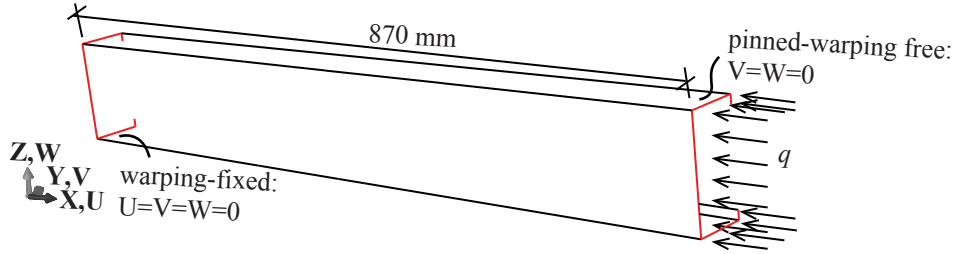
Figure 5: Example I: dimensions and loading/boundary conditions.

Reconstructed modal amplitudes and participations along the member are retrieved by using Eq. (14) and Eq. (16) and shown in Figure 6. The error of the reconstructed out-of-plane displacement field is 0.08% according to Eq. (21). Local mode 7 is dominant as shown in Figure 6 and the variation of its amplitude in Figure 6a is consistent with the buckling shape in Figure 8. For member-wise out-of-plane displacement participation, they read $P_7 = 70.9\%$ and $P_5 = 24.9\%$ by using Eq. (22). Distortional buckling occurs (mode 5) and mixes with local buckling. The strain energy decomposition is conducted per Eq. (17) as shown in Figure 7, where the grid (i, j) indicates the strain energy stored in the interaction of mode i and j. The total strain energy is computed to be $1518.8 N \cdot mm$ according to Eq. (18), comparing to ABAQUS yielding of $1468.4 N \cdot mm$ (3.4% difference). It is confirmed that energy-wise mode 7 dominates as it contributes to 94.2% of the strain energy.
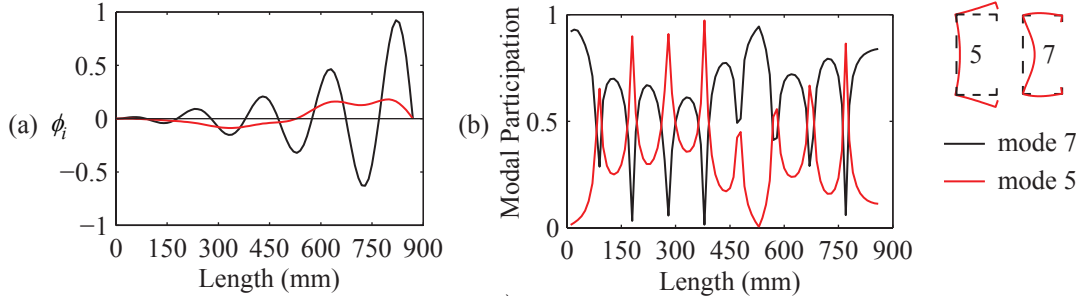
Figure 6: Example I: GBT buckling mode amplitudes and modal participation: local buckling along the member.
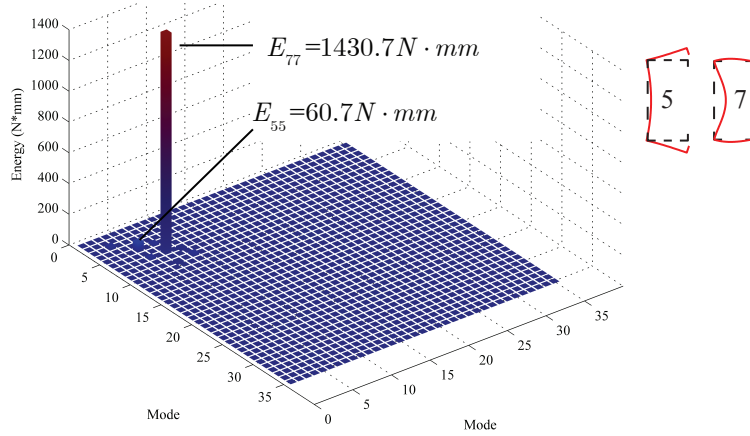
Figure 7: Example I: strain energy decomposition.

The bending stresses in the transverse and longitudinal directions are reconstructed by using Eq. (19) and Eq. (20) respectively. The results are compared with SFEA results in Figure 8 and Figure 9. In the comparison, SFEA transverse bending stress is read from ABAQUS from the cross-section top fiber positions, because the transverse membrane stress is negligible as assumed by GBT (Schardt, 1989). For SFEA result in the longitudinal direction, the bending stress is obtained by taking out the membrane stress from the stress at cross-section top fiber, i.e.,

$$\sigma_{xx-FE}^{F}(x,s) = \sigma_{xx-FE}(x,s,1/2t) - \sigma_{xx-FE}(x,s,0). \tag{25}$$

From Figure 8 and Figure 9, it can be seen the magnitude and distribution of reconstructed stress field are consistent with SFEA result. Because the reconstruction process uses the out-of-plane displacement field (V, W in Figure 1), it is hoped the method be used in conjunction with 3D displacement field measurement to analyze experimental point cloud in the future. Because small displacement is considered herein, the bending stress and displacement field can decomposed into modal contributions and the transverse bending as shown in Figure 10. For this example the transverse bending stress is dominated by mode 7 (local).
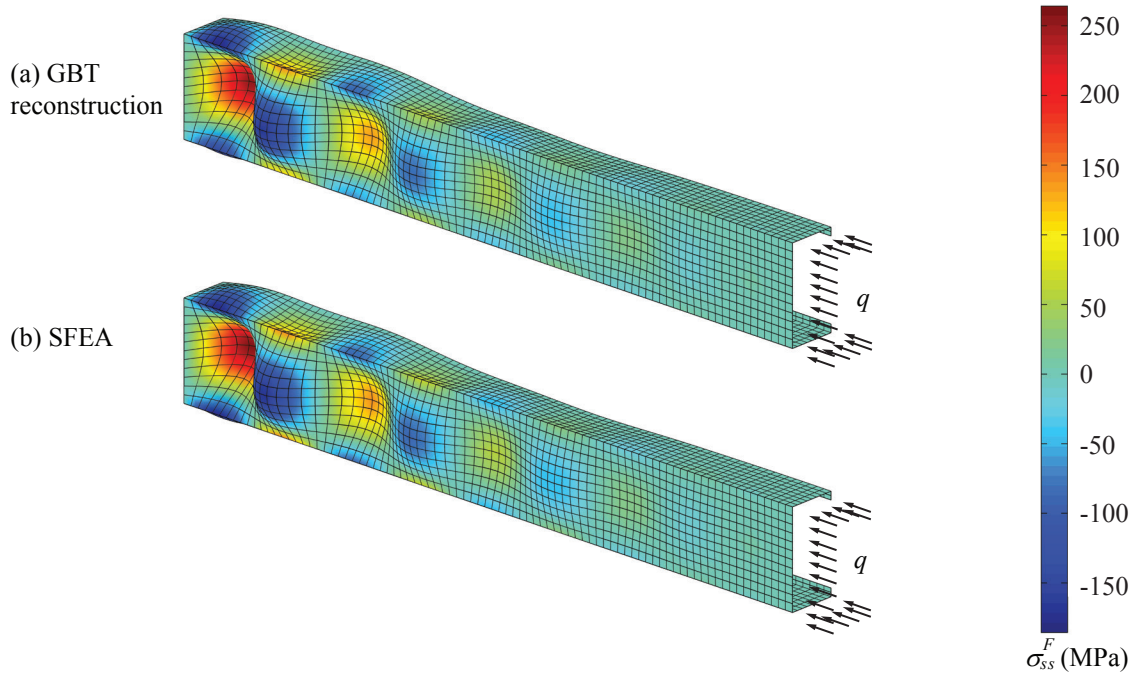
11

Figure 8: Example I: Transverse bending stress comparison for prismatic member: (a) GBT reconstruction; (b) SFEA.
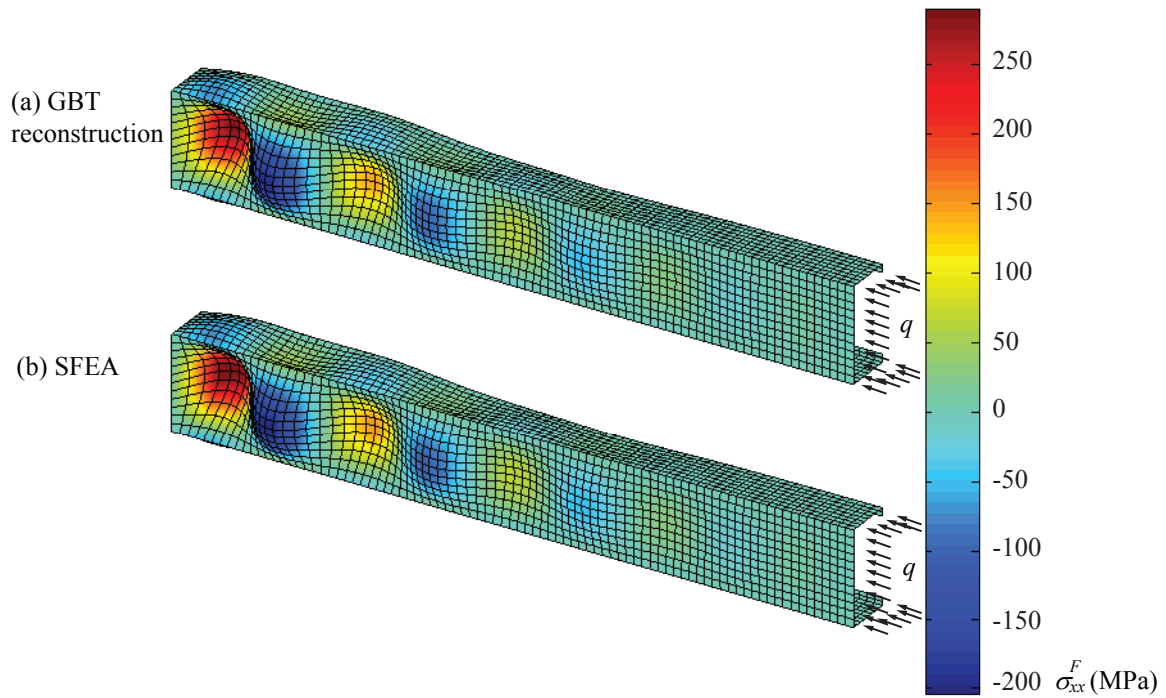

Figure 9: Example I: Longitudinal bending stress comparison for prismatic member: (a) GBT reconstruction; (b) SFEA.
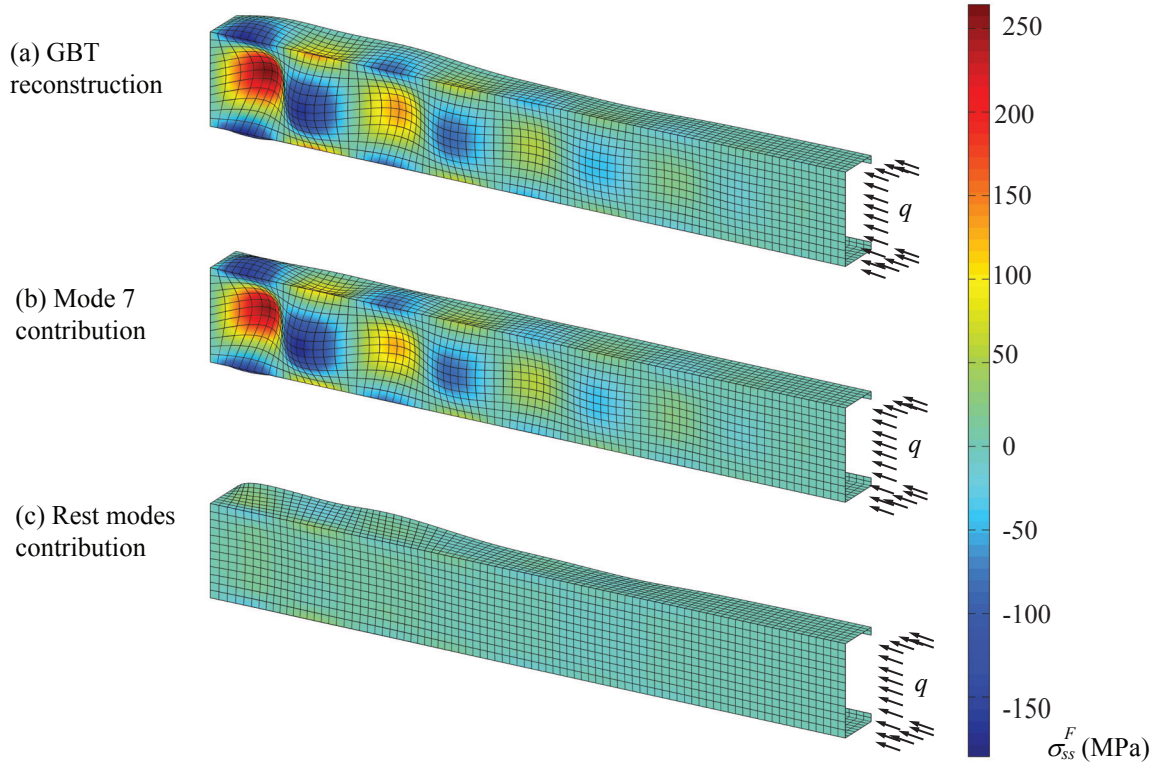
Figure 10: Example I: Transverse bending stress decomposition: (a) GBT reconstruction; (b) contribution from mode 7 and (c) contribution from other modes.

4.2. Example II

The second example involves a $1260\,mm$ long member pinned-warping free at both ends and loaded at both ends by uniform compression, and warping is prevented from mid-length cross-section in Figure 11. The cross-section and material properties are identical to the previous example.
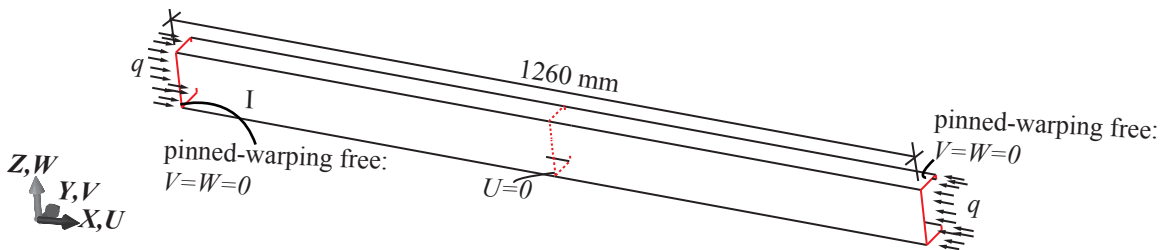

Figure 11: Example II: dimensions and loading/boundary conditions.

The first mode buckling load calculated by GBT is $146.6\,kN$. Modal amplitude and participation along the member are presented in Figure 12. It is shown the dominant GBT mode is local buckling (mode 7) mixing with symmetric distortional buckling mode 5, and the variation of ϕ_7, ϕ_5 agree with the mode shape in Figure 12, Displacement field error by Eq. (21) is calculated to be 0.07%. Using Eq. (22), the member-wise displacement participation read $P_7 = 64.2\%$ and $P_5 = 31.8\%$ for mode 7 and 5 respectively. From strain energy perspective, the total strain energy is computed to be $3149.2N \cdot mm$, comparing to ABAQUS reading of $3032.2N \cdot mm$ (3.9% difference). Mode

13

7 is responsible for 93.9% of the total energy (Figure 13). Transverse and longditudinal bending stress are also retrieved by using Eq. (19), Eq. (20) respectively and shown in Figure 14, Figure 15. The reconstructed bending stress field are consistent with that read from SFEA.
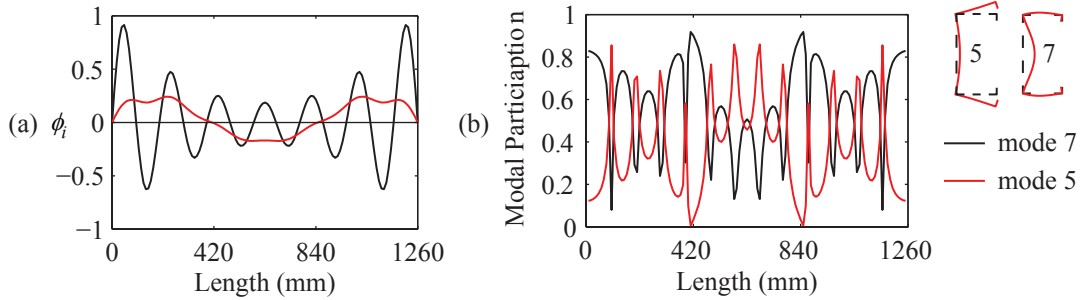

Figure 12: Example II: GBT buckling mode amplitudes and modal participation: local buckling along the member.
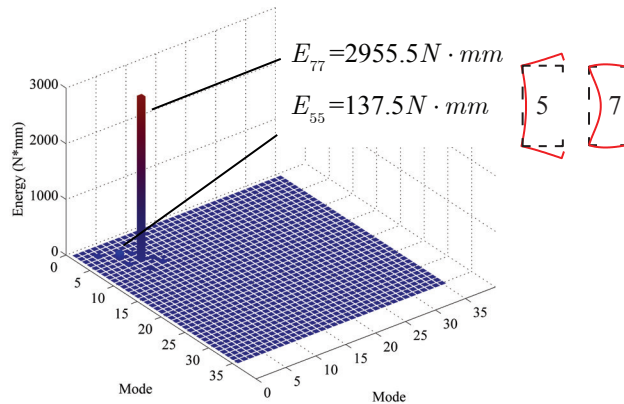

$$E_{77}=2955.5N\cdot mm$$

$$E_{55}=137.5N\cdot mm$$

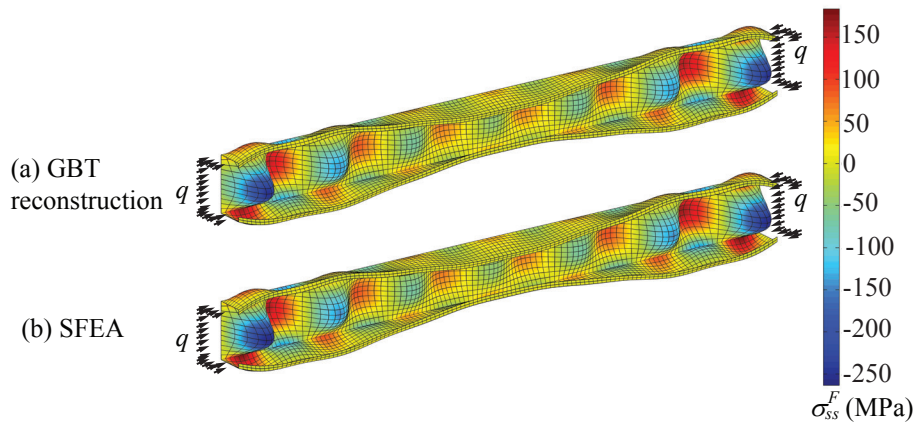Figure 13: Example II: strain energy decomposition

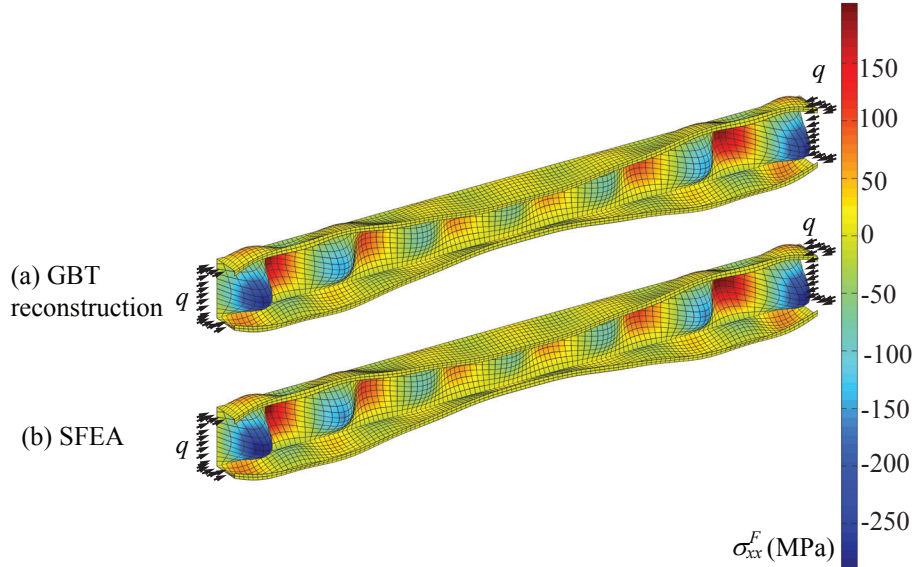Figure 14: Example II: Transverse bending stress comparison: (a) GBT reconstruction; (b) SFEA.

14

Figure 15: Example II: Longditudinal bending stress comparison: (a) GBT reconstruction; (b) SFEA.

5. Conclusions and future work

Buckling mode decomposition of normalized displacements, bending stresses, and strain energy from any thin-walled structure 3D deformation surface (point clouds, finite element results) is performed with GBT. Normalized displacement field, bending stress components and strain energy can all be reconstructed with quantitative participation known that can be useful for future design approaches. The method first extracts GBT modal amplitudes at discrete cross-sections and then reconstructs the continuous modal amplitude field piece-wisely using polynomials. The normalized displacement field, bending stresses and strain energy are all retrieved and decomposed using GBT modal amplitude field and associated GBT constitutive laws. Two examples are provided and the results are validated against SFEA results. The errors are minimum reading 0.08% and 3.4% (displacement and energy) for Example I and, 0.07% and 3.9% (displacement and energy) for Example II. The authors are now working on method to exploit the modal decomposition in design.

References

Abambres, M., Camotim, D., and Silvestre, N. (2014). "Modal decomposition of thin-walled member collapse mechanisms." *Thin-Walled Structures*, 74, 269–291.

Ádány, S. (2014). "Flexural buckling of simply-supported thin-walled columns with consideration of membrane shear deformations: Analytical solutions based on shell model." *Thin-Walled Structures*, 74, 36–48.

Ádány, S., Joó, A. L., and Schafer, B. W. (2010). "Buckling mode identification of thin-walled members by using cFSM base functions." *Thin-Walled Structures*, 48(10-11), 806–817.

Cai, J. and Moen, C. D. (2015). "Automated Buckling Mode Identification of Thin-walled Structures from 3d Mode Shapes or Point Clouds." *Proceedings of the Annual Stability Conference*, USA, Nashville, TN.

Camotim, D., Silvestre, N., Gonçalves, R., and Dinis, P. B. (2004). "GBT analysis of thin-walled members: new formulations and applications." *Thin-walled structures: recent advances and future trends in thin-walled structures technology*, 137–168.

Dinis, P. B. and Camotim, D. (2011). "Local/distortional/global mode interaction in simply supported cold-formed steel lipped channel columns." *International Journal of Structural Stability and Dynamics*, 11(05), 877–902.

Gonçalves, R., Ritto-Corrêa, M., and Camotim, D. (2010). "A new approach to the calculation of cross-section deformation modes in the framework of generalized beam theory." *Computational Mechanics*, 46(5), 759–781.

Lama-Salomon, A., Tao, F., Cai, J., and Moen, C. D. (2015). "Buckling mode identification for a cold-formed steel column experiment with 3d image-based reconstruction." *Proceedings of the Annual Stability Conference*, USA, Nashville, TN.

Li, Z., Ádány, S., and Schafer, B. (2013). "Modal identification for shell finite element models of thin-walled members in nonlinear collapse analysis." *Thin-Walled Structures*, 67, 15–24.

Nedelcu, M. (2012). "GBT-based buckling mode decomposition from finite element analysis of thin-walled members." *Thin-Walled Structures*, 54, 156–163.

Schafer, B. W. (2008). "Review: the direct strength method of cold-formed steel member design." *Journal of constructional steel research*, 64(7), 766–778.

Schardt, R. (1989). *Verallgemeinerte technische biegetheorie*. Springer, Berlin.

Silvestre, N. and Camotim, D. (2002). "Second-order generalised beam theory for arbitrary orthotropic materials." *Thin-Walled Structures*, 40(9), 791–820.

Silvestre, N. and Camotim, D. (2003). "Nonlinear generalized beam theory for cold-formed steel members." *International Journal of Structural Stability and Dynamics*, 3(04), 461–490.

Silvestre, N. and Camotim, D. (2013). "Shear Deformable Generalized Beam Theory for the Analysis of Thin-Walled Composite Members." *Journal of Engineering Mechanics*, 139(8), 1010–1024.